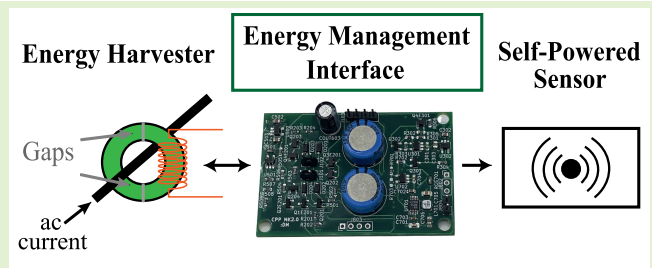


Rule the Joule: An Energy Management Design Guide for Self-Powered Sensors

Daniel Monagle¹, Graduate Student Member, IEEE, Eric A. Ponce¹, and Steven B. Leeb¹, Fellow, IEEE

Abstract—Energy harvesters present the exciting opportunity to create sensor nodes that can power or recharge themselves. Given the intermittent nature of available ambient energy for these harvesters and the common discrepancy between the harvested power and average power required to operate a sensor load, electronic energy management interfaces between the harvester source and a sensor load are often necessary. This article presents a design methodology for energy management interfaces between energy harvester sources and sensor loads. The design guide is practically demonstrated through the prototyping of a low-power energy management module that interfaces a clampable, split-core current transformer (CT) magnetic energy harvester (MEH) to an off-the-shelf bluetooth low energy (BLE) embedded hardware sensor kit. This article documents the design and experimental performance of the cold-start, energy harvest enhancement, overvoltage protection, and energy distribution control capabilities of this energy management interface. The experimental results demonstrate successful cold-start using discrete logic, average power harvest enhancements up to nearly 400% under certain harvester voltage load conditions, and a hysteretic control method for servicing an approximately 50 mW sensor load.

Index Terms—Energy harvesting, energy management, maximum power point tracking (MPPT), saturation, sensor interface electronics, split-cores, wireless sensor nodes.



I. INTRODUCTION

THE growth of the Internet-of-Things (IoT) and wireless sensor networks (WSNs) markets demands innovation in energy harvesting and energy management for these systems. With over 11 billion IoT-connected devices worldwide as of 2021 [1], designers must create solutions that efficiently store energy and manage power flow in energy harvesters and sensor nodes. Energy harvesters allow for batteryless sensor operation. Harvester source power, however, may be limited compared to desired sensor power needs.

Existing thermoelectric [2], piezoelectric [3], [4], [5], [6], photovoltaic [7], [8], vibration-based electromagnetic [9], and current transformer (CT) magnetic energy harvesters (MEHs) [10], are examples of energy harvester designs that often employ additional circuitry for maximizing power harvest capabilities or for efficiently converting harvester source voltages to an appropriate level for a downstream load. These

various harvesting systems naturally differ with respect to instantaneous and average power density, size, system complexity, and energy availability in the harvester installation environment [11]. Efficient interface circuitry is often added between the harvester itself and a sensor node. Interface circuitry manages system startup, ac-dc and dc-dc conversion, energy storage, maximum power point tracking (MPPT), and energy flow between the harvester and a sensor node. Several existing works have explored what is often referred to as “power management modules” or an “energy-aware interface” to manage these functions [4], [5], [6], [7], [8], [9], [12], [13].

Some existing works, particularly those targeting harvester systems dependent on weather patterns, adopt a predictive system based on historical energy harvest events for intelligently scheduling energy distribution to loads [14], [15]. These systems, however, are subject to poor performance or failure when the model predictions are inaccurate. In this article, a dynamic energy management circuit senses and controls energy flow continually during operation, contributing to system robustness in the face of unexpected high or low energy harvest conditions.

Recent advances in energy management for sensing solutions include [16], [17], [18], [19], [20]. Sultania and Famaey [16] demonstrated a batteryless bluetooth low energy (BLE) prototype with a commercial power management module (e-peas AEM10941) for supplying power to a Nordic BLE sensor kit. As the AEM10941 performed MPPT for a solar cell

Manuscript received 22 September 2023; revised 19 November 2023; accepted 19 November 2023. Date of publication 4 December 2023; date of current version 2 January 2024. This work was supported by the Office of Naval Research Structural Acoustics Program and The Grainger Foundation. The associate editor coordinating the review of this article and approving it for publication was Dr. Yongjia Li. (Corresponding author: Daniel Monagle.)

The authors are with the Department of Electrical Engineering and Computer Science, Massachusetts Institute of Technology, Cambridge, MA 02139 USA (e-mail: monagled@mit.edu; eaponce@mit.edu; sbleeb@mit.edu).

Digital Object Identifier 10.1109/JSEN.2023.3336529

and managed energy flow to the BLE sensor kit, the authors used experimentally determined power consumption of various BLE tasks to create an energy-aware sensor node that executed specific tasks according to specific energy storage thresholds [16]. Wright et al. [17] developed a flux-funneling inductive energy harvester, explored the effects of varying resistive loading conditions on harvested power, and employed a series compensating capacitor to cancel the harvester source reactance and enhance power output. Yeh et al. [18] demonstrated magnetic-piezoelectric harvesters for self-powered temperature sensor nodes. Although the focus of [18] was the comparative performance of different magnetic-piezoelectric harvester mechanisms, the work also determined optimal resistive loading conditions for each harvester mechanism, and employed a LTC3588-1 commercial power management circuit that integrates rectification and dc-dc conversion circuitry and regulated power flow to a temperature sensor and wireless transmitter [18]. For a marine monitoring application, Carandell et al. [19] produced a kinetic energy harvester with an ADP5092 commercial power management unit that managed MPPT, startup, boost conversion, and both charging and protection of an energy storage stage [19]. While harvester source design is not the primary focus of this article, the study of optimal harvester loading conditions and energy enhancement strategies, like those explored in the references above and in our previous work [20], are essential to an informed energy management module design.

There are a wide variety of integrated commercial resources and discrete analog and digital solutions for constructing a state of the art energy management module. For example, in this work we employ a LTC3388-1 dc-dc converter between our energy management module's storage stage and the power rail of the energy management microcontroller unit (MCU). This provides an efficient and necessary voltage conversion between the relatively high voltage of the energy storage stage compared to the desired 1.8 V MCU supply. Our proposed energy management module uses discrete MOSFETs, which are dynamically switched according to a MPPT algorithm that performs active rectification with carefully controlled timing based on the saturation of the harvester source, to rectify an ac harvester output into the dc energy storage stage. Alternatively, the LTC3588 used in [18] integrates rectification and dc-dc conversion into a single integrated circuit (IC). Such integration forgoes the efficiency benefits of an active rectification method for the elegance of an integrated power management unit that simplifies the system design and can help minimize system size and cost, which are relevant, practical constraints for self-powered sensors. To the authors' best knowledge, a commercially available integrated solution that provided the capabilities for both the dynamic protection method and the specific MPPT method described in this work, was unavailable. Our proposed system demonstrated below could be an excellent candidate for future integration efforts.

This article serves as a design guide for energy management in any self-powered sensor. The energy management design for a self-powered sensor system highlights three major features.

- 1) Cold-start capability.
- 2) Efficient energy conversion and storage.

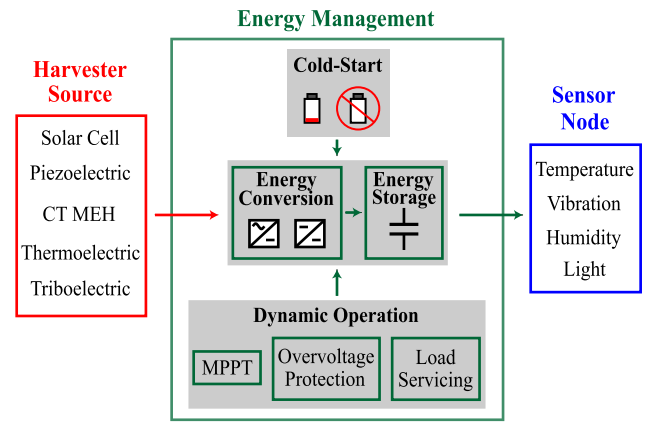


Fig. 1. Any self-powered system must appropriately interface between a harvester source and sensor node. Major design components include cold-start circuitry to boot the system up from a depleted state, efficient energy conversion and storage units, and dynamic algorithms for MPPT and other energy enhancement techniques, overvoltage protection, and servicing a sensor node.

3) Algorithms for dynamic operation.

An overview of the key design blocks for a general self-powered system is shown in Fig. 1. This article discusses the general design challenges and processes associated with each of the three major design features, while also demonstrating a specific prototype energy management module that serves as a design example.

This design guides spans “passive” and “active” modes of energy management module operation, employing low power discrete analog circuitry often used in the existing literature, while also incorporating the benefits of a dedicated MCU and digital control. The novelty of this work is emphasized in the comprehensive self-powered sensor system performance, where the proposed energy management module self-starts with discrete glue logic, drastically enhances energy harvest with a MPPT algorithm over a wide harvester output voltage range, services a wireless sensor node, and dynamically protects itself against overvoltage events due to surplus energy harvesting transients.

This article demonstrates the design and experimental performance of an ultralow power energy management system for a split-core CT MEH sensor node. The split-core energy harvester clamps around an ac current-carrying conductor and harvests energy from the surrounding magnetic fields. The system presented in this article consists of power electronic circuitry and digital control for implementing a power harvest enhancement technique that exploits and times the saturation of the magnetic core [21] as well as a hysteretic control method for regulating power flow to a sensor node.

II. SYSTEM OVERVIEW

Fig. 2 shows the illustrative example used to demonstrate the design guide presented in this article. While the techniques for energy management described in this article are generally applicable toward any self-powered sensor system, this work illustrates a systematic design procedure with a split-core CT MEH. This MEH presents interesting challenges and opportunities for startup, energy harvest enhancement,

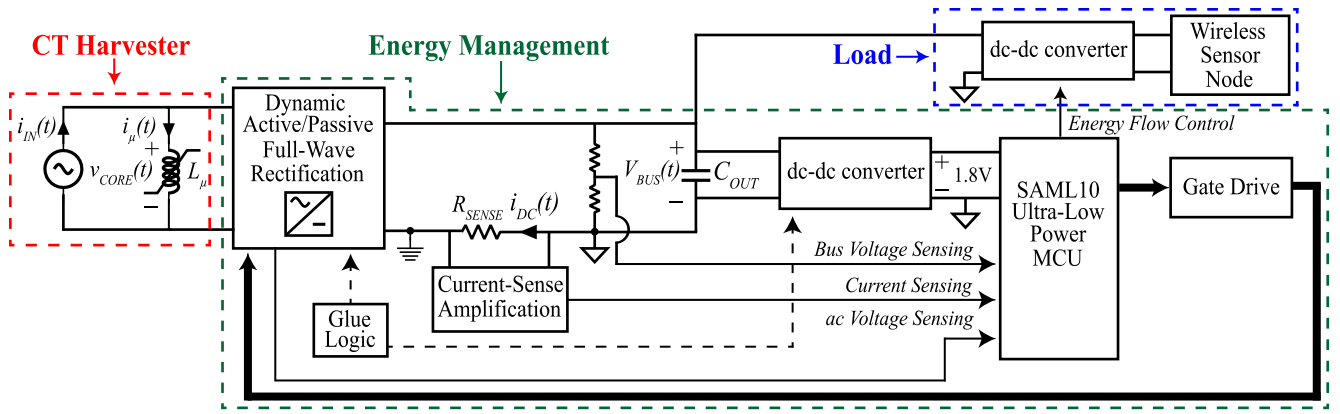


Fig. 2. High-level system diagram of the self-powered sensor node designed and evaluated in this article. The system is categorized into an equivalent circuit model for the energy harvester, the power electronic and embedded circuitry required for energy management, and a sensor load which includes a dc-dc converter stage.

and overvoltage protection. The CT MEH is wound with several, often hundreds, of turns of wire that are referred to as the CT “secondary” winding. The CT harvester core clamps around a single turn of an ac current-carrying conductor, often referred to as a “primary” wire. Voltage is produced at the CT secondary winding according to Faraday’s Law of induction. This harvester is represented by an equivalent secondary-side circuit model consisting of an ac current source in parallel with a nonlinear, saturating magnetizing inductance. The ac current source in this equivalent circuit model carries a current

$$i_{IN}(t) = \frac{I_P}{N} \sin(\omega t) \quad (1)$$

where I_P is the amplitude of the current flowing in the primary wire, often expressed in rms value, N is the number of turns of the secondary winding, and ω is the frequency of the primary wire current in radians per second.

The energy management system interfaces the harvester secondary winding to a sensor load. This energy management interface includes dynamically controlled rectification circuitry, dc voltage and current sensing for use in an energy harvest enhancement algorithm and overvoltage protection, discrete glue logic for handling startup conditions, dc-dc converter stages, a comparator used as a gate driver, and a MCU to manage energy flow throughout the system and to service a wireless sensor load.

The energy management circuitry of a self-powered system must be carefully designed to consume as little power as possible. Furthermore, the circuitry must be able to self-start, especially in cases like those explored in this work, where a battery is not present at all in the system. Table I includes conservative power consumption estimates of key system elements within our proposed energy management system according to manufacturer’s specification sheets. $P_{PASSIVE}$ refers to the estimated power consumption of each system block in the startup state, where V_{BUS} is less than our chosen 3 V threshold to transition into “active” operation. The passive state power consumption values therefore assume a nominal, conservative 3 V condition on V_{BUS} . P_{ACTIVE} refers to the estimated power consumption of each system block in the “active” state, which, as will be demonstrated in the experimental performance

TABLE I
ESTIMATED POWER CONSUMPTION OF PROPOSED ENERGY MANAGEMENT SYSTEM

System Component	$P_{PASSIVE}$ [μ W]	P_{ACTIVE} [μ W]
Glue Logic	42.5	573
Current-Sense Amplification	277	108
1.8V dc-dc and MCU	2.4	1710
Gate Drive	18.6	52
Miscellaneous	4.5	31.5
TOTAL	345 μW	2.47 mW

section of this article, operates around a nominal V_{BUS} of approximately 8 V. The “Miscellaneous” row of Table I refers to the estimated power consumption of necessary resistive dividers that provide level shifting between, for example, the system bus voltage and the MCU input put used for sampling the bus voltage. As will be demonstrated experimentally in Section VI of this article, our energy management module harvests nearly 100 mW under a 7.0 A rms primary current excitation. Thus, the total estimated active power consumption of the energy management module is approximately 2.5% of the total energy harvest under such conditions.

Our existing work has proposed an analytical model for predicting the power harvest capabilities of a CT MEH design [22]. This article focuses on the design and performance of the energy management interface circuitry controlling power flow between the harvester source and sensor load.

The system operates in its passive state during startup, using discrete, ultralow power logic to ensure the capacitive energy storage C_{OUT} can charge to an acceptable level before enabling downstream circuitry like the dc-dc converter powering the MCU. Once the capacitive energy storage is sufficiently charged, the system switches into its active state during which the power supply for the MCU is enabled, and the MCU begins to perform energy enhancement and management tasks. A flowchart of the system state machine is shown in Fig. 3.

III. COLD-START CAPABILITY

An energy harvesting sensor system can be considered “self-powered” as long the average energy harvested into the system is greater than or equal average energy dissipated and

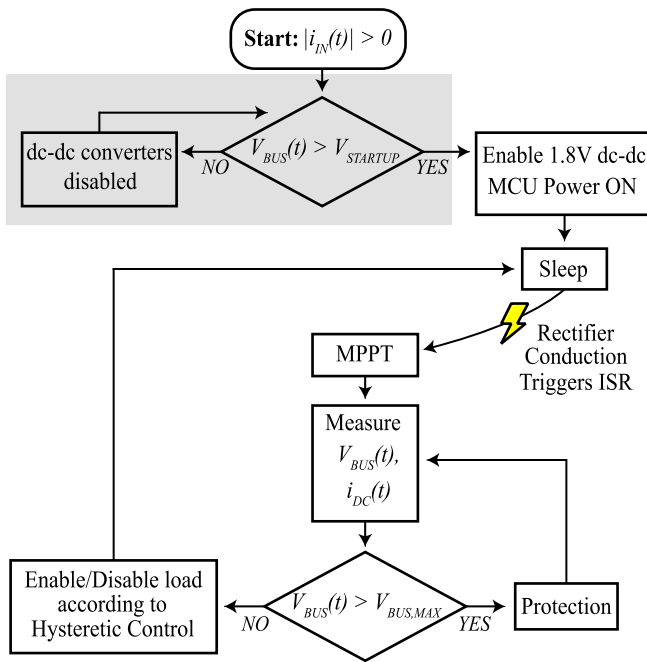


Fig. 3. Software flowchart that describes our system’s cold-start capabilities, active control for MPPT and load servicing during operation, and overvoltage protection. The shaded region denotes the system in passive operation. The system is event-driven, waking the MCU from an ultralow power sleep state to perform active control duties using interrupt service routines (ISRs).

consumed by the system. This qualification does not exclude battery-powered systems, provided that the battery is recharged with harvested energy greater than or equal to the energy it delivers when servicing the system. The addition of a rechargeable battery to a self-powered sensor system can be extremely useful for delivering quick, large bursts of current during power-hungry sensor operations, such as data transmission from a wireless sensor node. Furthermore, widely available, lithium-polymer (LiPo) batteries often exhibit nominal voltages exceeding 3.7 V, significantly simplifying system startup, as the charged battery can initially provide the necessary voltage levels and power to enable energy conversion circuitry and MCU circuitry before any harvester has begun to harvest energy into the system. The addition of a battery, however, introduces essential design requirements like short-circuit and over/undervoltage protections. Batteries also generally have shorter total lifetimes than capacitors.

Completely batteryless, self-powered systems can rely on supercapacitors for energy storage. While this can significantly increase the serviceable lifetime of the self-powered unit, it presents the design challenge of booting up or cold-starting the energy management and sensor load circuitry from an initial state of zero stored charge. Efficient startup hardware must restrict downstream circuitry from draining power out of the capacitive energy storage until the supercapacitors have charged to a sufficient voltage level for maintaining some form of steady-state operation. Meanwhile, this startup hardware itself must reliably operate while the supercapacitor energy storage is undercharged. A network of discrete comparators, passive components, and switches can accomplish this task.

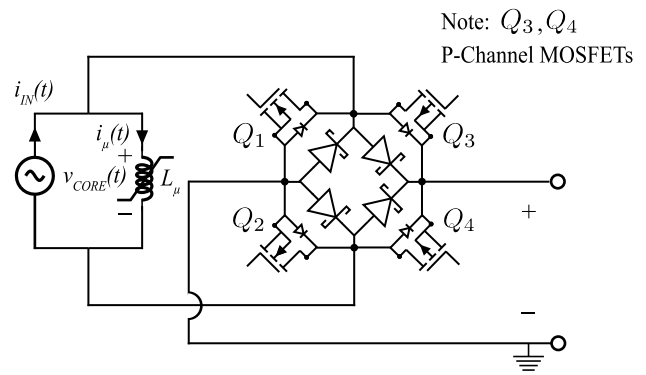


Fig. 4. Schottky diodes allow for passive conduction on startup, while the MOSFETs in parallel with each diode are then actively controlled to enhance power harvest once the MCU has been powered on.

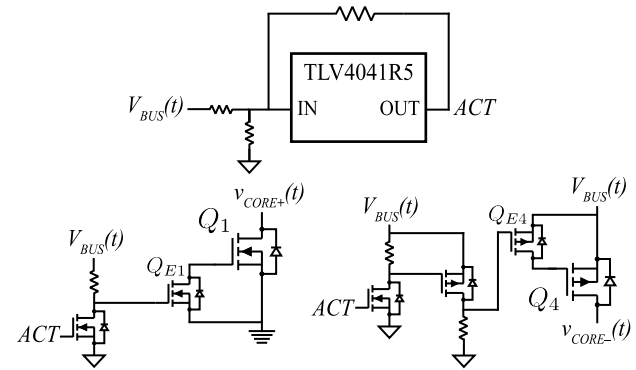


Fig. 5. TLV4041R5 comparator holds the ACT signal low until the C_{OUT} capacitor has charged to a sufficient state, after which point downstream circuitry and the MCU are enabled.

In terms of the system designed in this work and referencing Fig. 2, the C_{OUT} capacitor voltage, $V_{BUS}(t)$, must be allowed to rise to a large enough level that both meet the minimum input voltage requirements of downstream dc-dc converters and ensures there is enough energy stored in C_{OUT} to service the startup current draw of the circuitry on the energy management module. Capacitor C_{OUT} receives charge from the ac current produced by the CT harvester, after that current has been rectified in the full-wave rectification stage.

The hardware used to rectify the ac voltage produced by the harvester core to the dc voltage V_{BUS} across C_{OUT} is shown in Fig. 4. The rectification stage consists of a full-bridge of Schottky diodes, each in parallel with a MOSFET that will be used for active rectification once the system has entered its “active” state. The MCU provides the logic signals for controlling each MOSFET in the rectifier, and a MAX934 comparator is used as a gate driver for level shifting the 0 to 1.8 V logic signals from the MCU to 0 to V_{BUS} logic for driving the MOSFET gates directly. During startup, however, the MCU is disabled and neither the logic level signals from the MCU nor the MAX934 outputs that will eventually be essential for energy enhancement during active operation are driven to a reliable on or off state.

Ultralow power glue logic, therefore, is employed to ensure that the circuitry used for active energy management is disabled. A hardware overview of the glue logic is shown in Fig. 5. The glue logic relies on discrete comparators to ensure

that MOSFETs in the full-wave rectification stage are held in an off-state during startup and that downstream dc-dc converters are disabled so that they do not draw excessive current from the C_{OUT} storage stage. A TLV4041R5 comparator IC provides a power-on-reset (POR) feature which holds the comparator output low when the device supply voltage V_S is less than its minimum startup voltage. The output of this comparator is referred to as the “active” (ACT) signal. Since the rectifier MOSFET gate signals are not driven to a reliable known state by the MAX934 during startup, four additional “enable” MOSFETs Q_{E1} through Q_{E4} are used to disable the rectifier MOSFETs Q_1 through Q_4 while ACT is low. The enable MOSFET hardware configuration is shown in Fig. 5 for N-channel MOSFET Q_1 and P-channel MOSFET Q_4 . Q_2 and Q_3 , not pictured in Fig. 5, have analogous hardware configurations to Q_1 and Q_4 , respectively, differing only in their positions within the full-bridge rectifier. This circuitry holds the rectifier MOSFETs in a proper off-state so that the rectifier can conduct through the full-bridge of Schottky diodes until ACT goes high and the MOSFETs can be controlled by the MCU. This glue logic strategy trades off loading V_{BUS} during “passive” startup versus during “active” operation. Employing these enable MOSFETs, instead of conventional pullup or pulldown resistors on the rectifier MOSFET gates, reduces the load on V_{BUS} while the ACT signal is low, promoting the system’s ability to self-start. This strategy does continually load V_{BUS} with resistors once ACT has gone high, however, this is less of a concern during “active” operation since energy harvest enhancement algorithms afford us the luxury of dissipating a minor amount of energy through the pullups and pulldowns in the glue logic.

Control signal ACT remains low until V_{BUS} exceeds a minimum startup voltage threshold, $V_{STARTUP}$, chosen by the designer. Once the ACT signal is high, the “enable” FETs Q_{Ei} are turned off by the glue logic, and a dc-dc converter which provides the power rail for the SAML10 MCU is enabled. The disabling of the Q_{Ei} MOSFETs and the enabling of the 1.8 V dc-dc converter for supplying power to the MCU allow the MAX934 to appropriately drive the rectifier MOSFET gates based on input signals provided by the now powered-on MCU.

IV. EFFICIENT ENERGY CONVERSION AND STORAGE

The energy management interface between any harvester source and sensor node must efficiently convert and store energy. A given energy storage technology trades off storage capacity with physical size. The energy management module requires relatively large capacitance for storing sufficient energy to power itself and a sensor load, but the storage stage cannot be made too large such that the self-powered sensor system is physically impractical or invasive to install. A larger storage stage may also cause the system to exhibit an unacceptably long startup time. A harvester source will produce a range of output voltage levels corresponding to ambient energy availability. A designer can size a necessary capacitive energy storage stage according to a load power budget and expected nominal capacitor voltage range

$$E_{LOAD} \leq \frac{1}{2}C(V_H^2 - V_L^2) \quad (2)$$

where E_{LOAD} is the energy consumed by a load for a given operation, C is the required value of the capacitance, and V_H and V_L refer to the high and low levels, respectively, of the voltage across the capacitor as it discharges over the time period of the energy-consuming operation. These voltage levels may be strictly constrained according to the output voltage capabilities of an energy harvester source or the input voltage requirements of a downstream load. A designer might also actively regulate these voltages with a control scheme. In cases where energy harvest events are infrequent, a designer may need to model the leakage of the storage stage, which is a function of both the storage technology itself and the quiescent current draw of the energy management circuitry. This highlights the importance of designing efficient energy management systems that have low-leakage currents and the capability to self-start in cases where energy harvest is so infrequent that even the minor leakage from the storage stage over long periods of time causes the energy storage to deplete below the level sufficient for “active” operation.

To illustrate this design process, we can focus in to the specific self-powered system implemented in this work. A Cypress Infineon programmable system-on-chip (PSoC) 6 BLE Pioneer Kit (CY8CKIT-062-BLE) acted as the sensor load. This BLE sensor kit ran an example project that samples temperature data and reports temperature readings to an on-board E-Ink display or over a BLE connection to a mobile device. The sensor kit was measured to consume an average power of approximately 38 mW at a 3.3 V voltage supply. The total “Load” as defined in Fig. 2 consists of this PSoC load and a 3.3 V dc-dc converter which, according to the manufacturer’s specifications, demonstrates about, conservatively, 80% efficiency at a 12 mA current output provided to the PSoC. Thus, this system’s load consumes an average power P_{LOAD} of

$$P_{LOAD} \approx \frac{38 \text{ mW}}{0.8} = 47.5 \text{ mW}. \quad (3)$$

A hysteretic control method regulates the $V_{BUS}(t)$ voltage across the supercapacitor stage C_{OUT} between 7 and 8 V by enabling and disabling the load. Therefore, to operate this estimated load for 3 s

$$47.5 \text{ mW}(3 \text{ s}) \leq \frac{1}{2}C_{OUT}((8 \text{ V})^2 - (7 \text{ V})^2) \quad (4)$$

$C_{OUT} \geq 19 \text{ mF}$ is required.

Along with a properly sized energy storage capacitor, an energy management interface must efficiently convert energy. Some energy harvester sources produce a dc output, but this output will vary depending on ambient energy availability. Therefore, efficient dc-dc converter stages are required for stepping up or down the harvester source voltage to acceptable levels for downstream circuitry. Several other harvester sources, such as the CT MEH used in this work, produce ac voltage, which must be rectified into the capacitive energy storage stage. Schottky diodes, in parallel with actively controlled MOSFETs, enable an energy conversion stage of the energy management module that can manage startup properly while also providing essential hardware for reducing losses during “active” operation. This rectification

scheme is robust in the face of nonideal outputs from the harvester source. In the TWA example, this may involve the addition of filtering of the harvested current signal in order to both properly detect rectifier conduction and measure power harvest.

B. Dynamic Circuit Protection

In cases of high ambient energy availability, an energy management module capacitive storage stage may be in danger of overvoltage conditions. The management module must ensure that the voltage ratings of its supercapacitor storage unit or sensitive ICs are not exceeded under such high energy harvest conditions. This could, for example, be accomplished with a dedicated voltage supervisor IC, or digital logic which prevents the energy storage stage from charging during such high ambient energy conditions. Alternatively, the presence of a low-power MCU on-board an energy management interface provides great flexibility for accomplishing a variety of MPPT, power electronic control, and load servicing tasks. Given the valuable presence of an MCU in the energy management module, a designer can employ the MCU and any of its internal ADCs or comparators to provide circuit protection to the entire self-powered sensor system.

In our system, when employing TWA, operating the core at higher load voltages yields higher power harvests, but practical constraints arise to limit V_{BUS} so as to not damage ICs elsewhere in the system. Supercapacitors tradeoff energy density for voltage rating, and in our system, the 5.5 V maximum rating of each FYD0H104ZF 100 mF supercapacitor in our implemented storage stage sets an upper limit on V_{BUS} . Two of these capacitors have been stacked in series between V_{BUS} and ground in our implementation to give an approximate absolute maximum $V_{\text{BUS}} < 11$ V constraint, which is also the absolute maximum supply voltage rating of the MAX934 comparator. Active protection of the circuit by limiting the bus voltage is achieved in this system as described below. As referenced in Fig. 3, the MCU samples the bus voltage and current during every detection of a conduction window, which occurs at a rate of 120 Hz in our system given a 60 Hz sinusoid in the primary wire. The natural time constant of the C_{OUT} series stack of 100 mF supercapacitors is approximately

$$\tau \approx R_{\text{ESR}} C_{\text{OUT}} \approx 10 \text{ s} \quad (5)$$

since the ESR of the FYD0H104ZF supercapacitor used in our design is given as 100 Ω at 1 kHz according to the manufacturer's datasheet. The bus voltage is sampled at least once every conduction window at a frequency of 120 Hz, or, equivalently, every 8.3 ms. Given that 8.3 ms is significantly shorter than $\tau \approx 10$ s, one can reasonably linearize the capacitor constitutive relation

$$i_c \approx C \frac{\Delta v_c}{\Delta t} \quad (6)$$

where i_c is the current flowing into a capacitance, C is the capacitance value, Δv_c is the change in voltage across the capacitor, and Δt is some time duration during which that voltage change occurs. Considering the nominal V_{BUS} of

approximately 8 V during operation, a $\Delta v_c \geq 3$ V is unacceptable given the 11 V maximum bus voltage specification. Under the linearized approximation, we find $i_c \geq 18$ A for a $\Delta t = 8.3$ ms time-span is required to cause a $\Delta v_c \geq 3$ V across $C_{\text{OUT}} = 50$ mF.

Thus, our minimum sampling rate of 120 Hz is an acceptable sampling rate for measuring V_{BUS} , since our 300-turn split-core CT energy harvester will produce an $i_{\text{IN}}(t)$ that is (1/300) that of the primary wire. To produce i_{IN} waveforms at our CT secondary in the range of 10–20 A in amplitude would require several thousands of amperes flowing in the primary wire which is far outside of the roughly 1–100 A design target of this system. This example demonstrates the determination of a sampling rate to ensure dynamic circuit protection using our on-board MCU under large harvesting conditions. Such protection functions could be useful candidates for future power management integration efforts, especially for interfacing with harvester sources that potentially produce high-voltage outputs.

Upon sampling V_{BUS} at this acceptable rate, the MCU makes a protection check to see if $V_{\text{BUS}} > V_{\text{BUS,MAX}}$, where $V_{\text{BUS,MAX}} = 10$ V was chosen to give a sufficient volt of headroom below the 11 V absolute maximum rating. If the protection condition is met, the MCU sets the appropriate logic signals for the rectifier MOSFET gates to continually short the core secondary winding with MOSFETs Q_1 and Q_2 until V_{BUS} has returned to an acceptably safe level for harvesting to continue.

C. Load Servicing

Ultimately, the energy management module is responsible for ensuring that the system remains self-powered. A designer again has freedom in choosing the means through which a sensor load is serviced. In this work, the MCU regulates energy transfer between the supercapacitor storage bank and wireless sensor node through a hysteretic control scheme. Based on a desired, nominal V_{BUS} level, the MCU adjusts the state of a digital output pin which enables the dc-dc converter providing power to an off-the-shelf, commercial sensor kit.

VI. EXPERIMENTAL SYSTEM PERFORMANCE

The energy management interface described above was manufactured and tested to evaluate the system's capabilities for powering a sensor module. A split-core MEH was constructed with a 5.45 cm³ Coilcore nanocrystalline split-core wound with 300 turns for its secondary winding. The core was clamped around a single primary turn of a conductor carrying a 60 Hz sinusoidal current provided by a Hewlett Packard 6813 A ac power source. Voltage and current measurements were made using a Keysight InfiniiVision DSOX4154A oscilloscope. The amplitude of the primary current was varied in order to evaluate the energy management interface under lower and higher power harvest conditions.

A picture of the experimental setup is shown in Fig. 7, where the split-core has been clamped around a single turn of the primary wire. A close-up photograph of the energy management prototype printed circuit board (PCB) is shown in Fig. 8. Fig. 9 overlays the measured bus voltage and measured

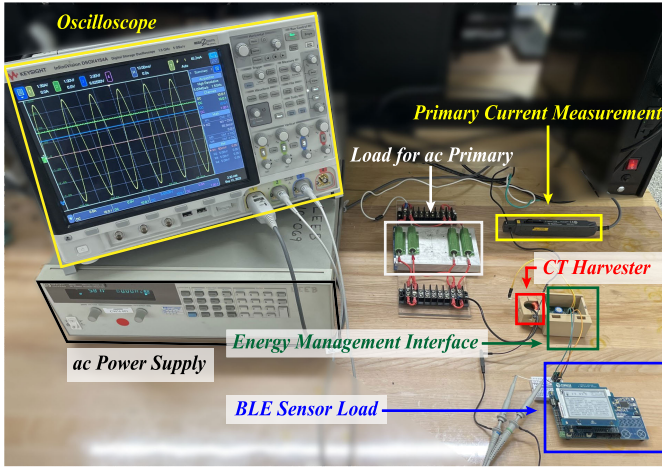


Fig. 7. Labeled photograph of the experimental setup, where the split-core CT harvester has been clamped around an ac power line, providing power to the energy management interface and BLE sensor kit.



Fig. 8. Photograph of the top side of the energy management PCB prototype with a United States quarter coin for scale reference.

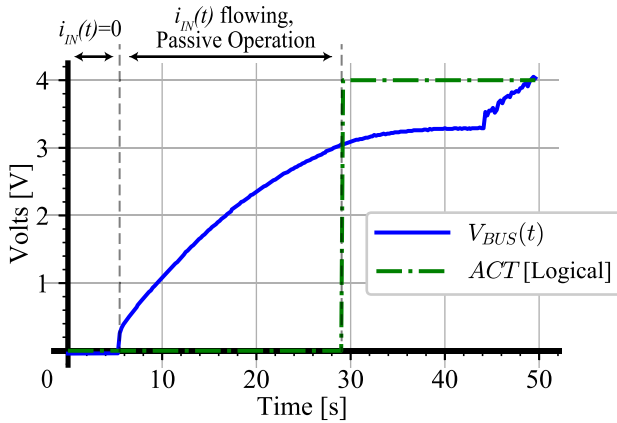


Fig. 9. Experimental performance of cold-start. MPPT kicks in shortly after the system has gone into active operation.

logical state of the ACT signal, demonstrating the system's successful cold-start with a 60 Hz 3.0 A rms primary current. As desired, the ACT signal remains low until $V_{BUS}(t)$ crosses a designer's chosen 3 V threshold enabling the dc-dc converter which provides a 1.8 V supply rail to the MCU.

Figs. 10 and 11 show the measured experimental performance and benefit of the energy harvest enhancement TWA control method under a 7 A rms primary current excitation. At an average $V_{BUS} \approx 6.0$ V, the system primary wire current and harvested dc current $i_{DC}(t)$ through R_{SENSE} were measured

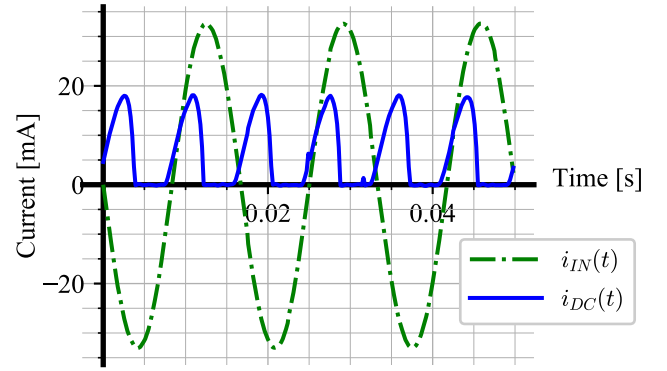


Fig. 10. Measured experimental harvested current without TWA algorithm running.

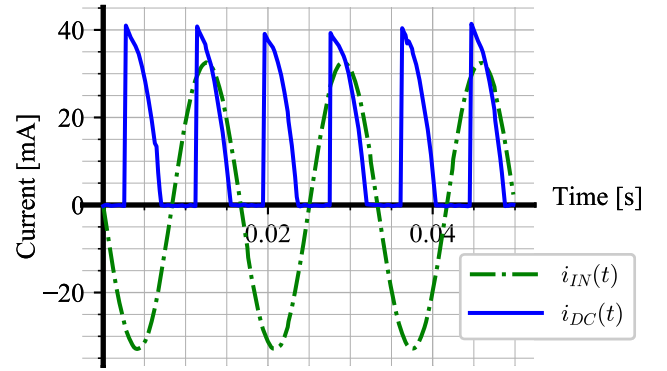


Fig. 11. Measured experimental harvested current with TWA algorithm running.

with and without the TWA energy enhancement scheme running. The $i_{IN}(t)$ waveform plotted in Figs. 10 and 11 is the measured primary current waveform divided by the turns ratio of the CT. It is clear from the experimental results that harvested dc current is significantly increased when TWA is implemented, as the timing of the harvester core saturation is manipulated such that the rectifier conducts close to the peak of the input current waveform. The average power harvest is described analytically

$$P_{OUT} = \frac{2}{T} \int_{t_{OPEN}}^{t_{CLOSE}} V_{BUS}(t) \cdot i_{DC}(t) dt \quad (7)$$

where T is the period of the input current waveform, $V_{BUS}(t)$ and $i_{DC}(t)$ are defined in Fig. 2, and t_{OPEN} and t_{CLOSE} refer to the start and end times, respectively, of the window during each half cycle of input current that $i_{DC} > 0$. The average power harvest was measured experimentally on the oscilloscope as the average of the product of $V_{BUS}(t)$ and $i_{DC}(t)$. Fig. 12 shows the measured average power harvest comparison over a wide sweep of average V_{BUS} levels with and without the system running TWA.

Fig. 12 shows experimental power harvest data under a primary current excitation of 7.0 A rms. As $V_{BUS}(t)$ charges and discharges over multiple volts at a timescale of seconds, $V_{BUS,AVG}$ refers to the average bus voltage on a cycle-by-cycle basis, which is relatively constant over several cycles of 60 Hz input current. Figs. 13 and 14 show $V_{BUS}(t)$ and the state of the MCU hysteretic control digital output pin, a signal we refer

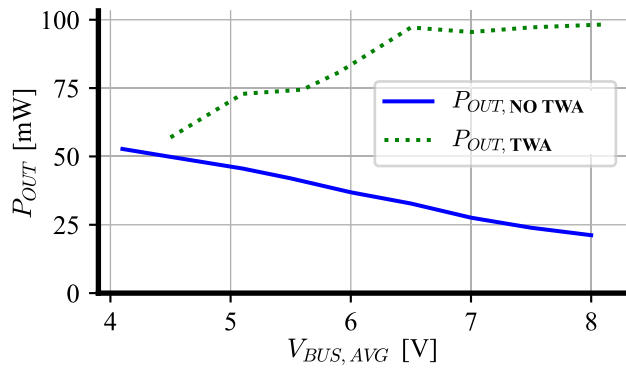


Fig. 12. Uncontrolled MEH system goes into deeper saturation at higher bus voltages and harvests less power, whereas TWA significantly increases power harvest at higher voltage levels.

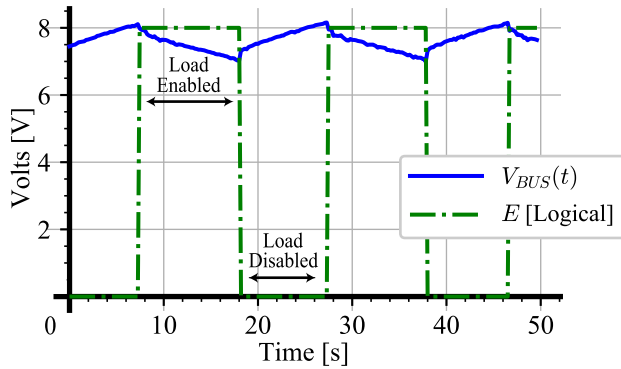


Fig. 13. Hysteretic control enables and disables the dc–dc converter and sensor node load according to bus voltage level. The implemented hysteretic controller enables the load when the bus voltage begins to exceed 8 V and disables the load when the bus voltage begins to drop below 7 V.

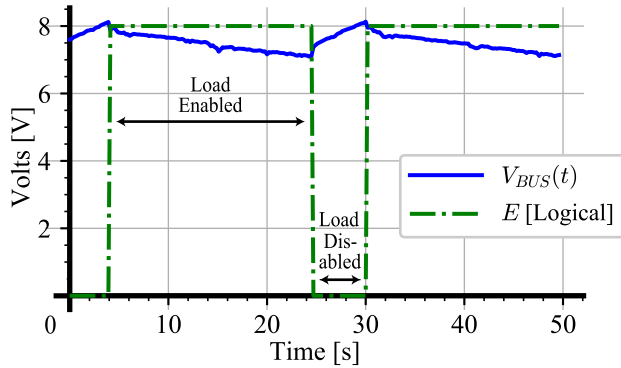


Fig. 14. At larger input currents, more power is harvested by the CT, and the duty cycle of the hysteretic control signal E is increased compared to that of Fig. 13.

to as E , under 60 Hz primary current excitations of 3.0 and 3.8 A rms, respectively. When E is high, the dc–dc converter providing power to the BLE sensor node is enabled. When E is low, the dc–dc converter for the BLE sensor kit is disabled, consequently disabling the sensor node.

Fig. 15 demonstrates the system’s protection capabilities. Under a 5.0 A rms primary current excitation, the average power harvest is greater than the consumption by the load, resulting in a $V_{BUS}(t)$ that is increasing even when E is high, enabling current flow to the dc–dc converter and PSOC

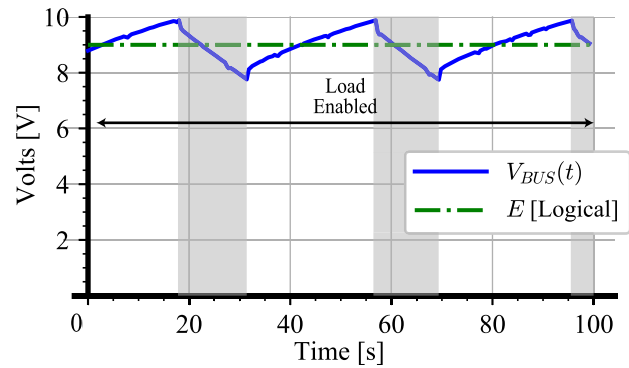


Fig. 15. At very high primary currents, the harvested energy is so great that the bus voltage increases even when the load is continually enabled. Shaded regions in this figure indicate time periods during which dynamic circuit protection prevents the bus voltage from exceeding 10 V by shorting the CT secondary.

sensor node. Once V_{BUS} reaches the $V_{BUS,MAX}$ threshold, the MCU turns on MOSFETs Q_1 and Q_2 to short the harvester core secondary winding, preventing C_{OUT} from charging to dangerous voltage levels. During this protection period, the load remains enabled and energy is discharged from C_{OUT} to the load until V_{BUS} returns to a safe threshold and harvesting is re-enabled.

VII. CONCLUSION

This article provides a design guide and framework for the energy management interface between an energy harvester source and a wireless sensor node. Design principles are demonstrated through the successful prototyping and operation of a magnetic energy harvesting self-powered sensor node. The energy management circuit documented in this work implemented cold-start functionality, MPPT techniques, overvoltage protection, and hysteretic control to power a BLE sensor kit, which continually sampled and reported temperature data over an E-Ink display.

ACKNOWLEDGMENT

The authors would like to thank LTJG Jacob Skimmons, USCG for his contributions to the mechanical clamping mechanism and enclosure for the energy harvester and energy management hardware. They also like to thank Dr. T. J. Rodgers Ph.D., Infineon, and Dr. Patrick Kane Ed.D.

REFERENCES

- [1] Statista. (2022). *Number of Internet of Things (IoT) Connected Devices Worldwide from 2019 to 2021, with Forecasts from 2022 to 2030*. Accessed: Jun. 12, 2023. [Online]. Available: <https://www.statista.com/statistics/1183457/iot-connected-devices-worldwide/>
- [2] C. Quintáns, J. Marcos-Acevedo, and C. Martínez-Peñalver, “Thermoelectric energy harvesting system based on water-stored energy and daily ambient temperature variations,” *IEEE Sensors J.*, vol. 20, no. 23, pp. 13919–13929, Dec. 2020, doi: 10.1109/JSEN.2020.2973452.
- [3] B. Zhao, J. Wang, W.-H. Liao, and J. Liang, “A bidirectional energy conversion circuit toward multifunctional piezoelectric energy harvesting and vibration excitation purposes,” *IEEE Trans. Power Electron.*, vol. 36, no. 11, pp. 12889–12897, Nov. 2021, doi: 10.1109/TPEL.2021.3083256.
- [4] Z. J. Chew, T. Ruan, and M. Zhu, “Power management circuit for wireless sensor nodes powered by energy harvesting: On the synergy of harvester and load,” *IEEE Trans. Power Electron.*, vol. 34, no. 9, pp. 8671–8681, Sep. 2019, doi: 10.1109/TPEL.2018.2885827.

- [5] T. Ruan, Z. J. Chew, and M. Zhu, "Energy-aware approaches for energy harvesting powered wireless sensor nodes," *IEEE Sensors J.*, vol. 17, no. 7, pp. 2165–2173, Apr. 2017, doi: [10.1109/JSEN.2017.2665680](https://doi.org/10.1109/JSEN.2017.2665680).
- [6] Z. J. Chew and M. Zhu, "Low power adaptive power management with energy aware interface for wireless sensor nodes powered using piezoelectric energy harvesting," in *Proc. IEEE SENSORS*, Nov. 2015, pp. 1–4, doi: [10.1109/ICSENS.2015.7370663](https://doi.org/10.1109/ICSENS.2015.7370663).
- [7] H. Kim, S. Kim, C.-K. Kwon, Y.-J. Min, C. Kim, and S.-W. Kim, "An energy-efficient fast maximum power point tracking circuit in an 800- μ W photovoltaic energy harvester," *IEEE Trans. Power Electron.*, vol. 28, no. 6, pp. 2927–2935, Jun. 2013, doi: [10.1109/TPEL.2012.2220983](https://doi.org/10.1109/TPEL.2012.2220983).
- [8] R. L. Rosa, C. Dehollain, A. Burg, M. Costanza, and P. Livreri, "An energy-autonomous wireless sensor with simultaneous energy harvesting and ambient light sensing," *IEEE Sensors J.*, vol. 21, no. 12, pp. 13744–13752, Jun. 2021, doi: [10.1109/JSEN.2021.3068134](https://doi.org/10.1109/JSEN.2021.3068134).
- [9] H. Liu, Z. Ji, T. Chen, L. Sun, S. C. Menon, and C. Lee, "An intermittent self-powered energy harvesting system from low-frequency hand shaking," *IEEE Sensors J.*, vol. 15, no. 9, pp. 4782–4790, Sep. 2015, doi: [10.1109/JSEN.2015.2411313](https://doi.org/10.1109/JSEN.2015.2411313).
- [10] J. Moon and S. B. Leeb, "Power electronic circuits for magnetic energy harvesters," *IEEE Trans. Power Electron.*, vol. 31, no. 1, pp. 270–279, Jan. 2016, doi: [10.1109/TPEL.2015.2401336](https://doi.org/10.1109/TPEL.2015.2401336).
- [11] O. B. Akan, O. Cetinkaya, C. Koca, and M. Ozger, "Internet of hybrid energy harvesting things," *IEEE Internet Things J.*, vol. 5, no. 2, pp. 736–746, Apr. 2018, doi: [10.1109/JIOT.2017.2742663](https://doi.org/10.1109/JIOT.2017.2742663).
- [12] T. N. Le, A. Pegatoquet, O. Berder, and O. Sentieys, "Energy-efficient power manager and MAC protocol for multi-hop wireless sensor networks powered by periodic energy harvesting sources," *IEEE Sensors J.*, vol. 15, no. 12, pp. 7208–7220, Dec. 2015, doi: [10.1109/JSEN.2015.2472566](https://doi.org/10.1109/JSEN.2015.2472566).
- [13] S. Chamanian, S. Baghaee, H. Ulasan, Ö. Zorlu, E. Uysal-Biyikoglu, and H. Külah, "Implementation of energy-neutral operation on vibration energy harvesting WSN," *IEEE Sensors J.*, vol. 19, no. 8, pp. 3092–3099, Apr. 2019, doi: [10.1109/JSEN.2019.2890902](https://doi.org/10.1109/JSEN.2019.2890902).
- [14] D. K. Sah, A. Hazra, R. Kumar, and T. Amgoth, "Harvested energy prediction technique for solar-powered wireless sensor networks," *IEEE Sensors J.*, vol. 23, no. 8, pp. 8932–8940, Apr. 2023, doi: [10.1109/JSEN.2022.3208730](https://doi.org/10.1109/JSEN.2022.3208730).
- [15] Y. Li, Z. Jia, and X. Li, "Task scheduling based on weather forecast in energy harvesting sensor systems," *IEEE Sensors J.*, vol. 14, no. 11, pp. 3763–3765, Nov. 2014, doi: [10.1109/JSEN.2014.2327221](https://doi.org/10.1109/JSEN.2014.2327221).
- [16] A. K. Sultania and J. Famaey, "Batteryless Bluetooth low energy prototype with energy-aware bidirectional communication powered by ambient light," *IEEE Sensors J.*, vol. 22, no. 7, pp. 6685–6697, Apr. 2022, doi: [10.1109/JSEN.2022.3153097](https://doi.org/10.1109/JSEN.2022.3153097).
- [17] S. W. Wright, M. E. Kiziroglou, and E. M. Yeatman, "Inductive power line harvester with flux guidance for self-powered sensors," *IEEE Sensors J.*, vol. 23, no. 18, p. 20474, Sep. 2023, doi: [10.1109/JSEN.2022.3225050](https://doi.org/10.1109/JSEN.2022.3225050).
- [18] P.-C. Yeh, T.-H. Chien, M.-S. Hung, C.-P. Chen, and T.-K. Chung, "Attachable magnetic-piezoelectric energy-harvester powered wireless temperature sensor nodes for monitoring of high-power electrical facilities," *IEEE Sensors J.*, vol. 21, no. 9, pp. 11140–11154, May 2021, doi: [10.1109/JSEN.2021.3056275](https://doi.org/10.1109/JSEN.2021.3056275).
- [19] M. Carandell, D. M. Toma, M. Carbonell, J. del Rio, and M. Gasulla, "Design and testing of a kinetic energy harvester embedded into an oceanic drifter," *IEEE Sensors J.*, vol. 20, no. 23, pp. 13930–13939, Dec. 2020, doi: [10.1109/JSEN.2020.2976517](https://doi.org/10.1109/JSEN.2020.2976517).
- [20] D. Monagle, E. Ponce, and S. B. Leeb, "Resonant circuits for split-core magnetic energy harvesters," *IEEE Trans. Ind. Electron.*, early access, Oct. 19, 2023, doi: [10.1109/TIE.2023.3323728](https://doi.org/10.1109/TIE.2023.3323728).
- [21] J. Moon and S. B. Leeb, "Enhancement on energy extraction from magnetic energy harvesters," in *Proc. IEEE Energy Convers. Congr. Expo. (ECCE)*, Montreal, QC, Canada, Sep. 2015, pp. 427–433, doi: [10.1109/ECCE.2015.7309720](https://doi.org/10.1109/ECCE.2015.7309720).
- [22] D. Monagle, E. Ponce, and S. B. Leeb, "Generalized analysis method for magnetic energy harvesters," *IEEE Trans. Power Electron.*, vol. 37, no. 12, pp. 15764–15773, Dec. 2022, doi: [10.1109/TPEL.2022.3195149](https://doi.org/10.1109/TPEL.2022.3195149).
- [23] N. Karami, N. Moubayed, and R. Outbib, "General review and classification of different MPPT techniques," *Renew. Sustain. Energy Rev.*, vol. 68, pp. 1–18, Feb. 2017, doi: [10.1016/j.rser.2016.09.132](https://doi.org/10.1016/j.rser.2016.09.132).
- [24] J. Moon and S. B. Leeb, "Analysis model for magnetic energy harvesters," *IEEE Trans. Power Electron.*, vol. 30, no. 8, pp. 4302–4311, Aug. 2015, doi: [10.1109/TPEL.2014.2357448](https://doi.org/10.1109/TPEL.2014.2357448).



Daniel Monagle (Graduate Student Member, IEEE) received the B.S. and S.M. degrees in electrical engineering and computer science from the Massachusetts Institute of Technology, Cambridge, MA, USA, in 2020 and 2022, respectively, where he is currently pursuing the Ph.D. degree.

His research interests include energy harvesting, magnetics, low-power circuit design, and self-powered systems.

Mr. Monagle was awarded the MIT School of Engineering 2023-2024 Thomas G. Stockham Jr. Fellowship for excellence in teaching and mentoring.



Eric A. Ponce received the B.S., M.Eng., and Ph.D. degrees from the Massachusetts Institute of Technology, Cambridge, MA, USA, in 2017, 2019, and 2023, respectively.



Steven B. Leeb (Fellow, IEEE) received the Ph.D. degree from the Massachusetts Institute of Technology, Cambridge, MA, USA, in 1993.

He has served as a Commissioned Officer in the USAF reserves, and he has been a member of the M.I.T. Faculty in the Department of Electrical Engineering and Computer Science, since 1993. He also holds a joint appointment in MIT's Department of Mechanical Engineering. He is the author or coauthor of over 200 publications and 20 U.S. Patents in the fields of electromechanics and power electronics.